

# Design of the AGIPD Sensor for the European XFEL

---

**J. Schwandt<sup>a,\*</sup>, E. Fretwurst<sup>a</sup>, R. Klanner<sup>a</sup> and J. Zhang<sup>a</sup>**

*<sup>a</sup>Institute for Experimental Physics, University of Hamburg  
Luruper Chaussee 149, D-22761 Hamburg, Germany  
E-mail: joern.schwandt@desy.de*

**ABSTRACT:** For experiments at the European X-Ray Free-Electron Laser (XFEL) the Adaptive Gain Integrating Pixel Detector (AGIPD) is under development. The particular requirements include a high dynamic range of 0, 1 to more than  $10^4$  photons of 12.4 keV per pixel within an XFEL pulse of less than 100 fs duration, and a radiation tolerance for doses up to 1 GGy for 3 years of operation. AGIPD is a hybrid-pixel detector system with a total of  $1024 \times 1024$  pixels of size  $200 \mu\text{m} \times 200 \mu\text{m}$ . AGIPD will use 16  $p^+n$ -silicon sensors of 500  $\mu\text{m}$  thickness. The nominal operating voltage is 500 V, however, for special applications operation close to 1000 V should be possible. Experimental data on the X-ray-dose dependence of the oxide-charge density and of the surface-current density have been implemented in the SYNOPSIS TCAD simulation program in order to optimize the design of the pixel and guard-ring layout. The methodology of the sensor design, the optimization of the most relevant parameters, and the optimized layout are described. Finally, the simulated performance, in particular the breakdown voltage, dark current and inter-pixel capacitance as function of the X-ray dose are presented.

**KEYWORDS:** XFEL; silicon pixel sensors; surface radiation damage; sensor simulation.

---

\*Corresponding author.

---

## Contents

<b>1. Introduction</b>	<b>1</b>
<b>2. X-ray radiation damage of segmented silicon sensors and TCAD simulation</b>	<b>1</b>
<b>3. Sensor optimization</b>	<b>3</b>
<b>4. Results of the sensor optimization</b>	<b>4</b>
4.1 Guard-ring structure	4
4.2 Pixel	6
<b>5. Summary</b>	<b>6</b>

---

## 1. Introduction

For experiments at the European X-Ray Free-Electron Laser (XFEL) the Adaptive Gain Integrating Pixel Detector (AGIPD) is under development [1, 2]. It is a hybrid-pixel detector system with  $1024 \times 1024$   $p^+$ -pixels of dimensions  $200 \mu\text{m} \times 200 \mu\text{m}$ , built of 16  $p^+n$ -silicon sensors, each with a sensitive area of  $10.52 \text{ cm} \times 2.56 \text{ cm}$  and a thickness of  $500 \mu\text{m}$ . The particular requirements include a dynamic range of 0, 1 to more than  $10^4$  photons of 12.4 keV per pixel for a pulse duration of less than 100 fs, negligible pile-up at the XFEL repetition rate of 4.5 MHz, and operation for X-ray doses up to 1 GGy in 3 years [3].

The paper describes the optimization of the AGIPD sensor, its final design and expected performance. After a short summary of results on X-ray radiation damage, the methodology of the optimization of the guard-ring structure and of the pixel layout using the SYNOPSIS TCAD [4] simulation program is presented. Finally, the optimized technological parameters and sensor layout, as well as the expected sensor performance, in particular the breakdown voltage, dark current and inter-pixel capacitance as function of X-ray dose are discussed. Based on the results of the simulations it is concluded that the AGIPD specifications can be met.

## 2. X-ray radiation damage of segmented silicon sensors and TCAD simulation

For 12.4 keV photons the maximum energy transfer to silicon atoms is well below the threshold energy of 21 eV for bulk damage [5]. Therefore, no bulk damage is expected, however surface damage will occur. The X-rays produce electron-hole pairs in the  $\text{SiO}_2$ . Whereas most of the electrons will leave the oxide, the holes, which have a much lower mobility than the electrons, will produce positive charges in the oxide or Si- $\text{SiO}_2$ -interface states [6].

In the case of a  $p^+n$  sensor the radiation-induced positive oxide charge will produce a sharp bending of the  $p^+$ -depletion boundary near the Si- $\text{SiO}_2$  interface, resulting in a high electric field

and a reduced breakdown voltage. In addition, an electron-accumulation layer forms, which prevents the depletion of the silicon below the SiO<sub>2</sub> and which causes an increase of the inter-pixel capacitance and charge losses.

The charge states of the Si-SiO<sub>2</sub> interface traps with energies in the Si-band gap depend on the trap type, their energies and the position of the Fermi level. They are responsible for the surface-generation current from regions where the Si-SiO<sub>2</sub> interface is depleted and thus exposed to an electric field.

Measurements on test structures (MOS capacitors and gate-controlled diodes) have been used to determine the dose dependence of the density of oxide charges  $N_{ox}$ , and the surface-current density  $J_{surf}$ . The results are shown in figure 1 [7, 8]. In order to obtain reproducible results after irradiation, the test structures had to be annealed for 10 minutes at 80°C [7]. It is found that  $N_{ox}$  increases with dose and saturates for doses above  $\approx 10$  MGy. The values for MOS capacitors from different vendors and for different crystal orientations show a spread of about a factor 2. In addition, annealing is observed already at room temperature [8].  $J_{surf}$  also increases up to  $\approx 10$  MGy and then drops to lower values. The reason for this drop is not understood and still under study.

The values which were used in the TCAD simulations are indicated in the figure as circles. In the simulations it was assumed that  $N_{ox}$  is uniformly distributed along the Si-SiO<sub>2</sub> interface. For the generation of the surface current the surface-recombination velocity  $s_0 = J_{surf}/(0.5 \cdot q_0 \cdot n_i)$  with the elementary charge  $q_0$  and the intrinsic charge-carrier density  $n_i$ , was used. Details on the models for the device simulation and for the scaling of the 2D results to 3D for the pixels, can be found in [9]. The breakdown voltage was determined by the criterion

$$\frac{dI}{dV} / \frac{I}{V} = 10,$$

with the gradient of the current-voltage curve  $dI/dV$ , and the ratio of the current to voltage  $I/V$ .

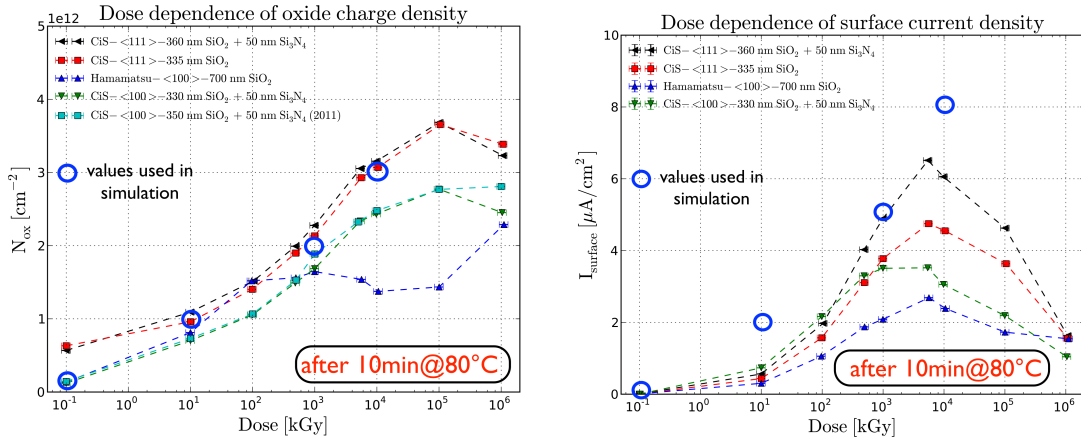


**Figure 1.** Dependence of the surface density of oxide charges (left) and surface-current density (right) on the X-ray irradiation dose for test structures (MOS capacitors, gate-controlled diodes) from different vendors after annealing at 80 °C for 10 minutes.

### 3. Sensor optimization

Based on detector and science simulations [10], the AGIPD collaboration has specified the sensor parameters to be achieved for doses from 0 to 1 GGy listed in table 1.

Parameter	Value
sensitive area	$10.52 \times 2.56 \text{ cm}^2$
mechanical thickness	$500 \pm 20 \text{ }\mu\text{m}$
distance pixel edges to cut edges	$1200 \text{ }\mu\text{m}$
resistivity of $n$ doping	$3 - 8 \text{ k}\Omega\cdot\text{cm}$
pixel dimensions	$200 \times 200 \text{ }\mu\text{m}^2$
operating voltage	$500 \text{ V}$
breakdown voltage	$> 900 \text{ V}$
coupling type	DC
inter-pixel capacitance@500V	$< 500 \text{ fF}$
total sensor dark current@500V	$< 50 \text{ }\mu\text{A}$

**Table 1.** Specifications for the AGIPD sensor for X-ray doses between 0 and 1 GGy

The parameters which have been optimized in the design of the sensor, some which are shown in figure 2, are for the pixels the gap, aluminum (Al) overhang and radius of  $p^+n$  junction and Al layer at the corners, for the guard-ring structure the number of rings, implantation widths, spacings and Al overhangs, and for the process parameters the depth of the junctions and the oxide thickness.

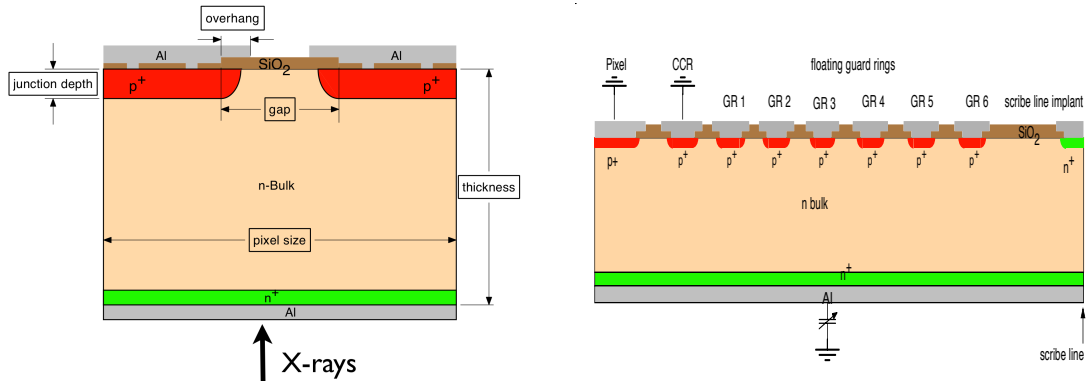


**Figure 2.** Left: Sketch of the sensor region simulated for the pixel optimization. Right: The region used for the guard ring simulation consists of half a pixel, the current collection ring (CCR), floating guard rings (GR - only 6 are shown) and the  $n^+$  scribe-line implant. Backplane and scribe-line implant are assumed to be on the same potential.

The performance parameters which have been optimized for doses between 0 and 1 GGy are the breakdown voltage, the leakage current and inter-pixel capacitance for the pixels, and the breakdown voltage and the voltage drop between the individual guard rings for the guard-ring structure. Moreover, it has been ensured that the depletion boundary does not touch the scribe line.

The strategy applied for the optimization can be summarized as follows:

- Guard ring (GR) optimization (2D simulations in (x,y) for the straight edges and in (r,z) for the corners):
  1. Optimize the breakdown voltage  $V_{bd}$  without guard ring (0 GR - only CCR) for different values of  $N_{ox}$  ( $5 \times 10^{10}$ ,  $10^{11}$ ,  $10^{12}$ ,  $2 \times 10^{12}$ , and  $3 \times 10^{12}$   $\text{cm}^{-2}$ ) as function of oxide thickness, junction depth and Al overhang.
  2. Estimate the number of floating GRs required for  $V_{bd} = 1000$  V.
  3. Vary the spacing between GRs, junction widths and Al overhangs, to achieve the maximum  $V_{bd}$  for a minimum width of the GR structure. This was achieved when the maximum electric fields in the gaps between the guard rings are approximately the same.
- Pixel optimization (2D simulations in (x,y)):
  1. Optimize the oxide thickness, Al overhang, gap and junction depth with respect to breakdown voltage, dark current and inter-pixel capacitance.
  2. Extrapolate the dark current and inter-pixel capacitances to 3D values.
  3. Check the breakdown voltage and dark current as function of voltage by a 3D simulation (only 1/4 pixel simulated).

## 4. Results of the sensor optimization

### 4.1 Guard-ring structure

The breakdown voltage  $V_{bd}$  without guard ring (0 GR) as function of oxide thickness  $d_{ox}$ , for different oxide-charge densities  $N_{ox}$ , two junction depths  $d_{jun} = 1.2$  and  $2.4$   $\mu\text{m}$  and an Al overhang of  $5$   $\mu\text{m}$ , is shown in figure 3. The breakdown voltages for  $N_{ox}$  values below  $10^{12}$   $\text{cm}^{-2}$  are above  $180$  V and are not shown. For  $N_{ox} = 10^{12}$   $\text{cm}^{-2}$  the values of  $V_{bd}$  increase from  $80$  V to  $150$  V when  $d_{ox}$  is increased. For higher  $N_{ox}$  values,  $V_{bd}$  reaches a maximum and then decreases. For  $N_{ox} = 3 \times 10^{12}$   $\text{cm}^{-2}$  the value of  $V_{bd}$  drops from  $70$  V at  $d_{ox} = 250$  nm, to  $20$  V at  $d_{ox} = 500$  nm. This sudden decrease of  $V_{bd}$  is related to the electron-accumulation layer below the Al overhang: If an accumulation layer is present, there is a single high-field region at the edge of the  $p^+n$  junction. Without accumulation layer the voltage drop occurs over the entire region below the Al layer, with one high field region at the edge of the junction and a second one below the end of the Al overhang. In addition, a deeper  $p^+n$  junction results in a lower field at the edge of the junction, thus further increasing the breakdown voltage.

From the curves of  $N_{ox} = 3 \times 10^{12}$   $\text{cm}^{-2}$  shown in figure 3, we conclude that the optimum value of the oxide thickness is  $230$  nm for a junction depth of  $1.2$   $\mu\text{m}$ , and  $270$  nm for  $2.4$   $\mu\text{m}$ . The corresponding breakdown voltages are between  $70$  and  $80$  V. This leads to the estimate that  $15$  floating GRs and a CCR are required to achieve a sensor-breakdown voltage of  $\approx 1000$  V.

After choosing a junction depth of  $2.4$   $\mu\text{m}$ , an oxide thickness of  $250$  nm, and performing step 3 of the GR-optimization procedure, the following parameters for the optimized guard-ring structure have been determined:

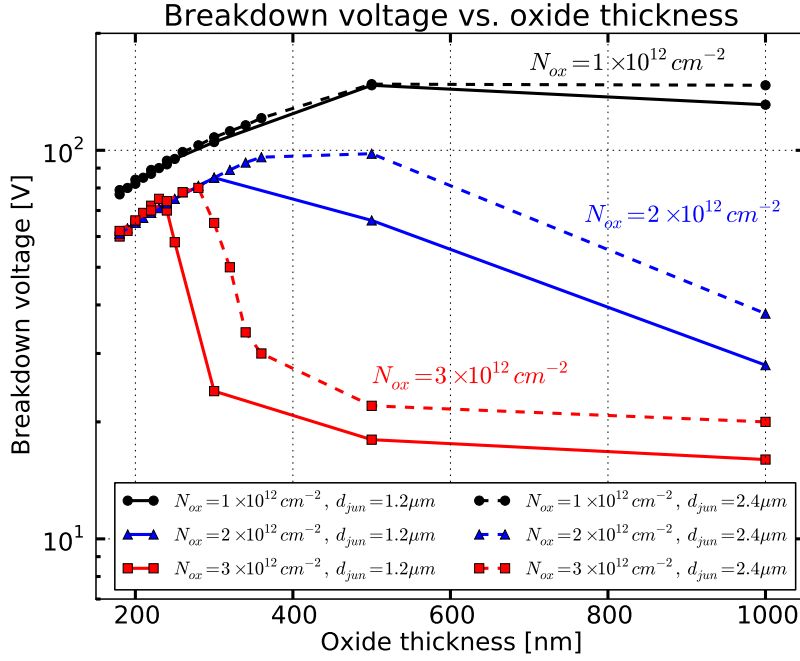


**Figure 3.** Breakdown voltage for 0 GR as function of the oxide thickness for different values of  $N_{ox}$ . The results are for a resistivity of  $5 \text{ k}\Omega\text{-cm}$ , an Al overhang of  $5 \text{ }\mu\text{m}$  and junction depths  $d_{jun}$  of  $1.2 \text{ }\mu\text{m}$  (solid) and  $2.4 \text{ }\mu\text{m}$  (dashed). The breakdown voltages for  $N_{ox}$  values below  $10^{12} \text{ cm}^{-2}$  are above  $180 \text{ V}$ .

- Gap between pixels and CCR:  $20 \text{ }\mu\text{m}$ .
- Width of the  $p^+n$  junction of the CCR:  $90 \text{ }\mu\text{m}$ .
- Al overhang of CCR:  $5 \text{ }\mu\text{m}$ .
- Gap between CCR and 1st GR:  $12 \text{ }\mu\text{m}$ .
- Widths of the  $p^+n$  junctions of the GRs:  $25 \text{ }\mu\text{m}$ .
- Al overhangs towards pixel for GRs 1-15:  $2, 3, 4, \dots, 16 \text{ }\mu\text{m}$ .
- Al overhangs away from pixel for GRs 1-15:  $5 \text{ }\mu\text{m}$ .
- Gaps between GRs 1-2, 2-3, ..., 14-15:  $12, 13.5, 15, \dots, 33 \text{ }\mu\text{m}$ .

A printout of the GDS file of the optimized guard-ring design is shown in figure 5 left. The simulated breakdown voltages  $V_{bd}$  of this structure for  $N_{ox}$  values of  $1 \times 10^{12}$ ,  $2 \times 10^{12}$  and  $3 \times 10^{12} \text{ cm}^{-2}$  and for different resistivities of the silicon are given in table 2. Shown are the results of 2D simulations in Cartesian coordinates (x,y) for the straight section of the guard rings, and in polar coordinates (r,z) for the corners. Given, that already  $\sim 600 \text{ 000}$  grid points are required for the 2D simulations, a 3D simulation of the guard-ring structure is not feasible. The results show that the minimum breakdown voltage is  $830 \text{ V}$  for a resistivity of  $3 \text{ k}\Omega\text{-cm}$  and  $N_{ox}$  of  $2 \times 10^{12} \text{ cm}^{-2}$ . The breakdown voltage is above  $900 \text{ V}$  for resistivities of  $5$  and  $8 \text{ k}\Omega\text{-cm}$ . Additional simulations

with  $N_{ox}$  of  $5 \times 10^{10} \text{ cm}^{-2}$  show that in the specified resistivity range of 3 to 8  $\text{k}\Omega\cdot\text{cm}$  the depletion region does not touch the scribe line for voltages below 990 V. With increasing  $N_{ox}$  the extension of the depletion region towards the scribe line decreases.

$N_{ox} [\text{cm}^{-2}]$	3 $\text{k}\Omega\cdot\text{cm}$		5 $\text{k}\Omega\cdot\text{cm}$		8 $\text{k}\Omega\cdot\text{cm}$	
	2D (x,y)	2D (r,z)	2D (x,y)	2D (r,z)	2D (x,y)	2D (r,z)
$1 \times 10^{12}$	> 1100 V	1060 V	> 1100 V	> 1100 V	> 1100 V	> 1100 V
$2 \times 10^{12}$	1000 V	830 V	1080 V	910 V	950 V	950 V
$3 \times 10^{12}$	1010 V	840 V	> 1100 V	910 V	1000 V	960 V

**Table 2.** Results of the 2D simulations in Cartesian and polar coordinates of the breakdown voltage as function of the surface density of oxide charges and bulk resistivity for the optimized guard-ring design.

## 4.2 Pixel

Because the pixel optimization is published in [9], here we only show that with above process parameters (junction depth of 2.4  $\mu\text{m}$ , oxide thickness 250 nm) and geometry parameters (gap of 20  $\mu\text{m}$ , Al overhang of 5  $\mu\text{m}$ , radius of junction of 10  $\mu\text{m}$  and radius of the Al layer of 12  $\mu\text{m}$ ) the specification of table 1 are met. A printout of the GDS file of the optimized pixel layout is shown in figure 5 right.

In figure 4 the I-V curves for 2D (x,y) simulations and for 3D simulations of a quarter of a pixel are plotted for the values of  $N_{ox}$  and  $J_{surf}$  given in table 3 for a resistivity of 5  $\text{k}\Omega\cdot\text{cm}$ . The currents are scaled to the pixel size of  $200 \times 200 \mu\text{m}^2$ . The breakdown voltage of the pixels for this design is above 1000 V. The difference in the voltage dependence of the currents between the 2D and the 3D simulations for high  $N_{ox}$  values is due to the shape of the electron-accumulation layer at the corners of the pixel: The surface current is given by the product of the surface-current density times the area of the depleted surface at the Si-SiO<sub>2</sub> interface. The corners of the pixels can only be properly simulated in 3D. The inter-pixel capacitance  $C_{int}$ , the sensor dark current  $I_{sensor}$  and the CCR dark current  $I_{CCR}$  are listed in table 3 for a voltage of 500 V and different  $N_{ox}$  values. All values are within the specifications.

$N_{ox}$ [ $\text{cm}^{-2}$ ]	$J_{surf}$ [ $\mu\text{A}/\text{cm}^2$ ]	$I_{sensor}$ [ $\mu\text{A}$ ]	$I_{CCR}$ [ $\mu\text{A}$ ]	$C_{int}$ [fF]
$1 \times 10^{12}$	2	7.4	0.6	120
$2 \times 10^{12}$	5	12.7	0.9	270
$3 \times 10^{12}$	8	14.4	1.2	312

**Table 3.** Simulated values of the inter-pixel capacitance  $C_{int}$ , the sensor dark current  $I_{sensor}$  and the CCR dark current  $I_{CCR}$  at 500 V.

## 5. Summary

Experimental results on the dose dependence of the surface density of oxide charges and the

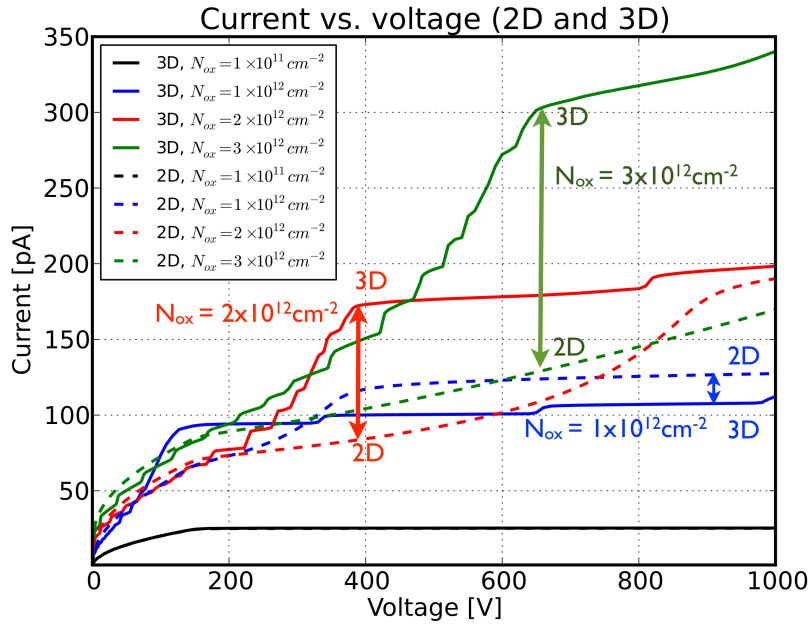


**Figure 4.** Comparison of the I-V curves for 2D simulations and for 3D simulations of a quarter of a pixel. The currents are scaled to a full pixel.

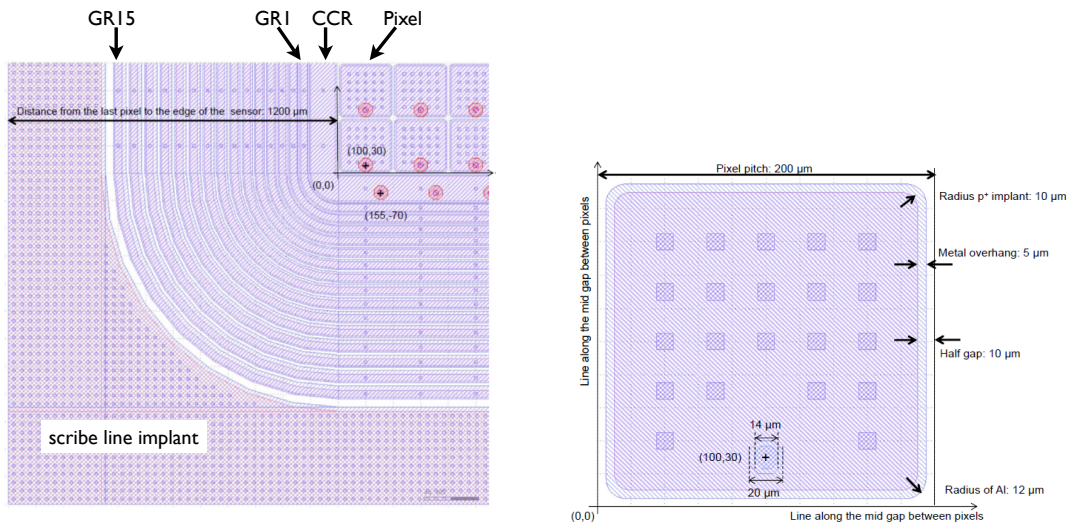


**Figure 5.** GDS printouts of the optimized layout of the AGIPD sensor. Left: From bottom left to top right one sees the scribe line, the scribe-line implant, the 15 guard rings (GR15 to GR1), the current-collection ring (CCR) and finally 6 pixels. Right: Pixel layout with the 21 vias which connect the Al to the  $p^+$  implant, and the opening in the oxide for bump bonding (center bottom). At the periphery, the edge of the  $p^+$ -implantion widow and the Al overhang can be seen.

surface-current density have been implemented in the SYNOPSIS TCAD simulation program and the design of the pixel and guard-ring layout for the AGIPD sensor has been optimized. The TCAD simulations show that the optimized sensor design meets the specifications for the AGIPD, in particular breakdown voltage, dark current and inter-pixel capacitance.

## Acknowledgments

This work was performed within the AGIPD Project financed by the European XFEL-Company. Additional support was provided by the Helmholtz Alliance *Physics at the Terascale* and J. Zhang was supported by the Marie Curie Initial Training Network *MC-PAD*. We thank the AGIPD colleagues for the excellent collaboration and the funding institutions for their support.

## References

- [1] M. Altarelli, et al., *European X-ray free electron laser technical design report, Technical Report*, The European XFEL, 2007.
- [2] B. Henrich et al., *The adaptive gain integrating pixel detector AGIPD, a detector for the European XFEL*, *Nucl. Instr. Meth. A* **633** (2011) S11-S14.
- [3] H. Graafsma, *Requirements for and development of 2 dimensional X-ray detectors for the European X-ray Free Electron Laser in Hamburg*, 2009 *JINST* **4** P12011.
- [4] Synopsys TCAD, webpage <http://www.synopsys.com/>.
- [5] A. Akkerman et al., *Updated NIEL calculations for estimating the damage induced by particles and gamma-rays in Si and GaAs*, *Radiat. Phys. Chem.* **62** (2001) 301.
- [6] T.R Oldham, *Ionizing Radiation effects in MOS Oxides*, World Scientific Publishing Co. (1999).
- [7] J. Zhang et al., *Study of radiation damage induced by 12 keV X-rays in MOS structures built on high resistivity n-type silicon*, *J. Synchrotron Rad.* **19** (2012) 340, arXiv:1107.5949.
- [8] J. Zhang et al., *Investigation of X-ray Induced Radiation Damage at the Si-SiO<sub>2</sub> Interface of Silicon Pixel Sensors for the European XFEL*, 14th International Workshop on Radiation Imaging Detectors, 1-5 July 2012, Figueira da Foz, Coimbra, Portugal, paper submitted and arXiv:1210.0427.
- [9] J. Schwandt et al., *Optimization of the Radiation Hardness of Silicon Pixel Sensors for High X-ray Doses using TCAD Simulations*, 2012 *JINST* **7** C01006, arXiv:1111.4901.
- [10] G. Potdevin, U. Trunk, H. Graafsma, *Performance simulation of a detector for 4th generation photon sources: The AGIPD*, *Nucl. Instr. Meth. A* **607** (2009) 51-54.